The International Journal of Advanced Manufacturing Technology (2024) 130:2313–2328
https://doi.org/10.1007/s00170-023-12766-3

ORIGINAL ARTICLE

Dynamic evolution behavior of cracks for single-track and multi-track clads in laser cladding

Yanhua Bian[1,2,3] · Binxin Dong[1,3] · Bo Chen[1,3] · Jianhao Guo[4] · Shaoxia Li[1,3] · Chongxin Tian[1,3] · Shouwen Xu[1,3] · Xiuli He[1,3] · Gang Yu[1,2,3]

Received: 13 September 2023 / Accepted: 24 November 2023 / Published online: 15 December 2023

Abstract

It is generally believed that the crack defect is the fatal issue that restricts the development of additive manufacturing technology. In this paper, Ni60 alloy coating on H13 surface is manufactured by laser cladding, and the dynamic evolution behavior of cracks during the process of single-track and multi-track overlapping cladding is studied. The morphology and microstructure characteristics of the coating and the crack initiation and propagation behavior are analyzed. The results show that the cracks mainly originate from the surface of the clad and propagate along the depth direction to the substrate. The laser power and scanning speed are the main factors that affect the crack behavior. With the increase of laser power, the process range for crack-free cladding is expanded. When the cladding speed is relatively low, the crack in the substrate can be initiated, and the crack propagates in the direction parallel to the laser scanning speed, which is manifested as the substrate being torn. The transverse cracks and the network-shaped cracks propagate continuously from single-track to multi-track cladding process. The crack-free cladding process can be achieved by a reasonable selection of processing parameters. This work aims to deeply understand the dynamic evolution behavior of cracks in laser additive manufacturing, and thus provide theoretical guidance for the crack-free cladding process.

Keywords Laser cladding · Additive manufacturing · Cracks · Residual stress · Thermal stress

Highlights
- The relationship between crack evolution behavior and process parameters has been established.
- The dynamic evolution behavior of crack has been analyzed from the single-track to multi-track overlapping cladding process.
- The mechanism for crack initiation and propagation in the substrate has been explained.

✉ Xiuli He
xlhe@imech.ac.cn

✉ Gang Yu
gyu@imech.ac.cn

[1] Institute of Mechanics, Chinese Academy of Sciences, No.15, North 4Th Ring West Road, Haidian District, Beijing 100190, China

[2] Center of Materials Science and Optoelectronics Engineering, University of Chinese Academy of Sciences, Beijing 100049, China

[3] School of Engineering Science, University of Chinese Academy of Sciences, Beijing 100049, China

[4] China Railway 14TH Bureau Groupment Shield Construction Engineering CO., LTD, Nanjing 210000, China

1 Introduction

H13 (4Cr5MoSiV1) hot working die steel is a chromium-molybdenum tool steel, which has been commonly used in the manufacture of extrusion dies, plastic molds, and casting dies [1]. During the working process, the surface of H13 mold suffers from an intense thermal-cold cycle load caused by the flow of high temperature metal, accompanied by wear, corrosion, and fatigue damage. Therefore, the surface strength of H13 steel is one of the key factors determining its life in engineering applications [2, 3]. Ni60A alloy is a Ni-based self-fluxing alloy with excellent properties of high hardness, oxidation resistance, and corrosion resistance, which has been widely applied in petroleum, chemical, and other industries [4, 5].

Laser cladding is one of the most promising additive manufacturing technologies, which can be used to manufacture the metallurgical bonding coating with excellent mechanical and chemical properties on the substrate [6–8]. The fundamentals of laser cladding are illustrated in Fig. 1. Employing laser cladding technology to manufacture Ni60

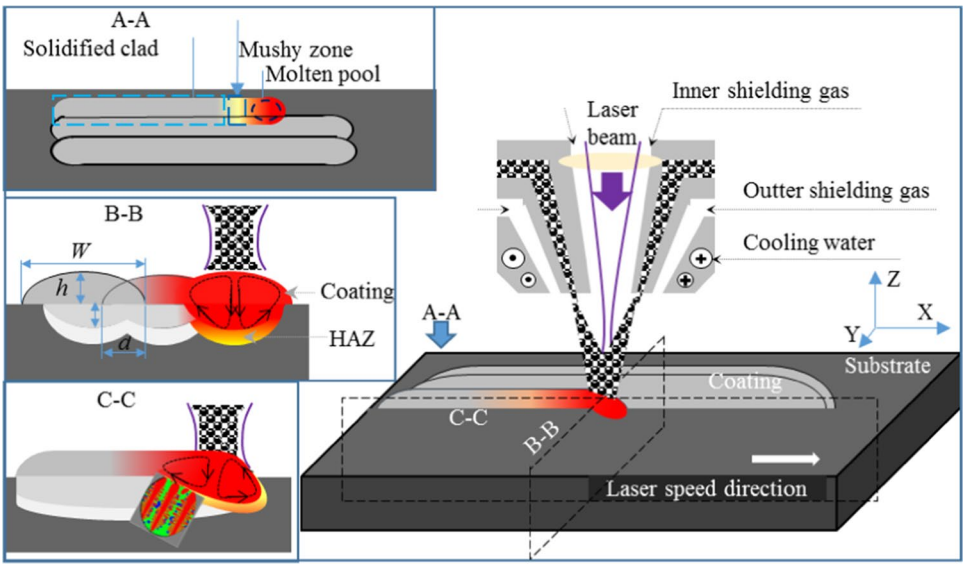

Fig. 1 Fundamentals of laser cladding

coating on H13 steel abrasive tools can effectively meet the high requirements for wear resistance and corrosion resistance of the abrasive tools [9, 10]. Wang et al. [9] used laser cladding technology to produce Ni60 samples on the H13 surface. They found that the refiner precipitates and larger amounts of the eutectics can increase the hardness of the H13 surface. Li et al. [10] employed the response surface methodology (RSM) analysis method to study the influence of cladding process parameters on the cladding morphology. The research results provided a theoretical basis for the morphology control and the optimization of process parameters in single-track laser cladding.

However, laser cladding is a non-equilibrium process accompanied by a high temperature gradient (10^5–10^6 K/m) and solidification rate (10^3–10^4 K/s), making the coating in a complex stress–strain state. Furthermore, the complex and interactional processing factors such as laser power, laser diameter, and defocus distance make the clad very sensibility to cracks. Meanwhile, the crack sensibility of the clad can also be enhanced by the brittle phases such as CrB, Cr_3Si, Ni_3B and other boride, and silicide eutectic compositions generated during the cladding process [11, 12]. Therefore, the generation of cracks has become the main limiting factor for the industrial applications of Ni60 alloy components manufacturing by laser cladding. The cracks generated in laser cladding process have been studied to some extent [13–15]. At present, the research on cracks in laser cladding is mostly carried out in the following three aspects: (1) analyzing the microscopic mechanism of crack initiation and propagation from the perspective of mechanics and material science, and proposing a description method of crack morphology; (2) simulating the temperature, temperature gradient, and stress distribution during laser cladding process to explain the behavior of crack generation and propagation; (3) establishing the relationship between process parameters and crack characteristics, and analyzing the rule of crack formation. According to reference [16], the basic reason for the coating susceptible to cracks was that the residual stress generated during the cladding process was higher than the fracture toughness of the coating. Zhou et al. [17] studied the law of crack initiation and propagation for Ni-based WC composite coatings. The results showed that cracks originated from the interface between the composite coating and the substrate, and the distribution of cracks was perpendicular to the direction of laser scanning speed and passed through the whole composite coating. The conditions for crack initiation, as well as its propagation behavior, can be revealed from the crack morphology. Therefore, the analysis of crack morphology is of great significance to reveal the crack formation mechanism, which is very important to control the generation of cracks. However, the dynamic evolution behavior of cracks from single-track to multi-track cladding process has never been studied. Huang et al. [18] investigated the relationship between the cracking behavior of Ni-based coating and the solidification characteristic of the molten pool. Lee et al. [19] measured the residual stress using the neutron diffraction method. Wang et al. [20] pointed out that the cyclic thermal stress in multi-layer overlay manufacturing could accelerate the crack initiation and propagation. Shi et al. [21] found that the crack rate of the Ni60A coating decreases with increasing line energy and decreasing powder feeding rate, and the crack distribution changes from network to parallel to no cracks. Zhang et al. [22] established a three-dimensional uncoupled thermomechanical finite element model to simulate the stress evolution in laser cladding and high residual stress was found at the second track and overlapping region. Sun et al. [23] employed the numerical simulation method to analyze the

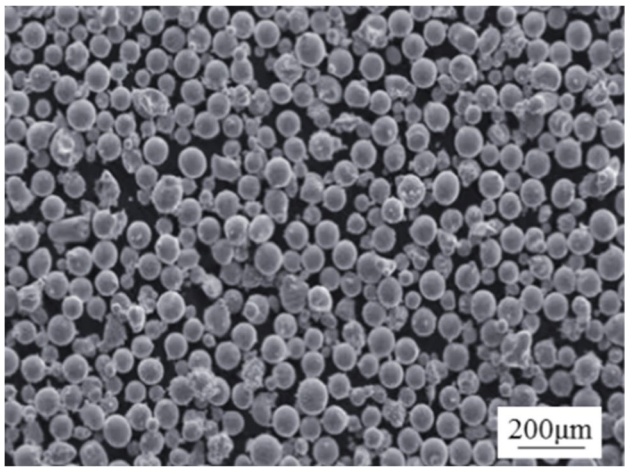

Fig. 2 Morphology of the Ni60 powder

temperature distribution of Ni60A clad. Nevertheless, few attempts have been made to investigation the cracks during laser cladding of Ni60 powder on H13 alloy. Furthermore, the initiation and propagation behaviors of cracks in the substrate have not been found in previous studies.

Therefore, in this paper, the dynamic evolution behavior of cracks in laser cladding process from single-track to multi-track overlapping is investigated, and the process parameters are optimized to effectively avoid the generation of cracks. First, the single-track cladding experiments are carried out, in which single processing parameters, namely laser power and laser scanning speed, are gradually changed. Second, the multi-track overlapping experiments are conducted using single-track process parameters under which there are no cracks or less cracks. The structural characteristics of cracks both on the surface and inside of the coating and substrate are analyzed. Furthermore, the dynamic evolution behavior and formation mechanism of cracks are discussed. This paper is helpful in promoting the understanding of crack formation mechanism in the process of laser additive manufacturing of Ni60 and provides a guidance for crack-free realization.

2 Experimental details

In this paper, the gas-atomized powder of Ni60 with particle size from 48 to 105 μm was used as the added material and its morphology is shown in Fig. 2. H13 alloy with the size of 40 mm × 40 mm × 10 mm was employed as the substrate. Table 1 shows the chemical composition of H13 and Ni60. Before the experiments, the substrate was cleaned with ethanol and then ground using a series of silicon carbide (SiC) paper of different grades (40 #–400#), and the powder was dried in a drying oven at 140 °C for 60 min and cooled at room temperature.

The IPG fiber laser system with a maximum output power of 10 kW and wavelength of 1070 nm was employed to carry out the cladding experiments. The defocus distance of laser spot to the substrate was set as 40 mm. A coaxial powder feeding nozzle was used and argon gas was employed as shielding and powder carrying gas. The flow rates of inner shielding gas, outer shielding gas, and powder carrying gas were set to be 15 L/min, 15 L/min, and 8 L/min, respectively. The detailed information of the nozzle structure can be obtained from our previously published paper [24]. The laser head, the nozzle, and other associated components were fixed to a 6-axis KUKA robot system.

To evaluate the dynamic evolution behavior of cracks in additive manufacturing process, single-track experiments with different laser powers and scanning speed were conducted and the experimental process parameters are listed in Table 2. Based on the surface morphology for the single-track laser cladding, the process parameters, under which there were no cracks or few cracks, were employed to conduct the multi-track overlapping experiments and the experimental process parameters are shown in Table 3. After laser cladding, all samples were ultrasonic cleaned with 95% ethanol for 30 min.

Table 2 Process parameters for single-track cladding

Processing parameters	Value
Laser power (W)	2000, 2500, 3000, 3500
Powder feeding rate (g/min)	5
Cladding speed (mm/s)	5, 10,15, 20, 25

Table 3 Process parameters for multi-track cladding

Processing parameters	Value
Laser power (W)	2500, 3000, 3500
Powder feeding rate (g/min)	5
Cladding speed (mm/s)	20
Overlapping rate (%)	30, 40

Table 1 Chemical composition (wt%) of H13 and Ni60

Alloy	Cr	C	B	Mo	V	Si	Mn	Ni	P	S	Fe
H13	5	0.42	–	1.27	0.88	0.89	0.3	0.16	0.021	0.008	Bal
Ni60	14	0.6	3.5	2.31	–	3.0	–	Bai	–	–	5.86

The Dino-lite digital microscope AM4115ZT with a magnification range from 20 × to 220 × was used to capture the surface morphology of the clad. The crack morphology inside the cladding layer was obtained by cutting the samples. The cut samples were then grounded using a series of silicon carbide (SiC) paper of different grades (240#–2000#) and polished using diamond suspensions for the preparation of metallographic sample. The polished samples were corroded using an etching solution of 100 mL HCl and 30 mL HNO_3, and subsequently washed with 99% ethanol. The optical microscope (MD-50 UM200i) and scanning electron microscope (ZEISS EVO18 Special Edition) were employed to observe the cross-sectional morphology of the clad, crack morphology both on the surface and inside of the clad, and microstructure of the clad.

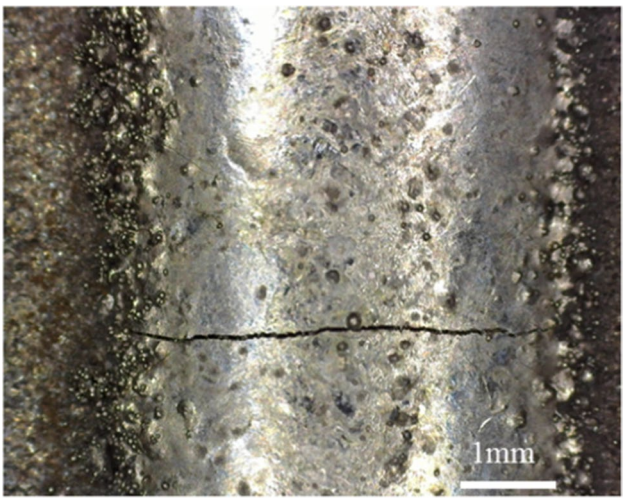

Fig. 4 Surface crack in single-track clad under larger magnification

3 Results and discussion

3.1 Morphology and characteristics of cracks in single-track clads

Laser cladding is a rapid melting and solidification process of metal materials, which involves complex physical phenomena such as heat, flow, and mass transfer behavior. The intricate physical process directly affects the morphology, microstructure, and crack behavior of the clad. Surface crack morphology in single-track clads and its surface morphology after dye penetration test are shown in Fig. 3. As can be seen from the larger magnification of the surface crack shown in Fig. 4, the surface crack initiates at the center of the clad and propagates along the width direction, and finally passes through the whole clad. Almost all the surface cracks are perpendicular to the laser scanning direction. Therefore, the initiation and evolution behavior of cracks inside the clad and the H13 substrate can be observed by cutting the sample along the direction parallel to the laser scanning speed.

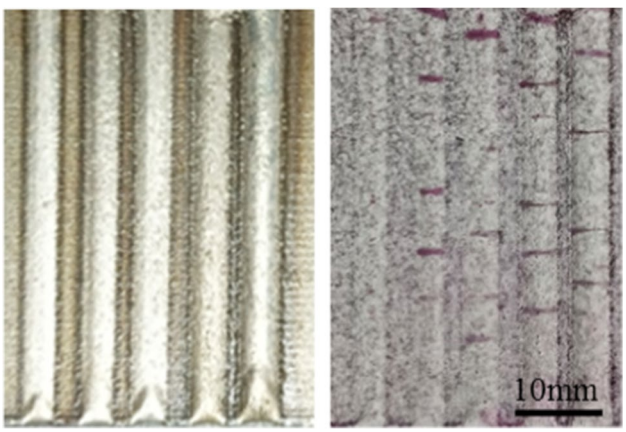

Fig. 3 Surface crack morphology in single-track clads

According to previous research, the main reason for crack development is the accumulation of residual stress in the coating [17]. The residual stress produced in the cladding process mainly includes two aspects: contraction stress and thermal stress. When the residual stress is higher than the fracture toughness of the coating, cracks initiate and propagate in the clad.

From the A-A view shown in Fig. 1, the single-track clad can be roughly divided into three zones: solidified clad, mushy zone, and molten pool. Right below the laser irradiation, a molten pool is formed on the H13 substrate, and the metal powder heated by the laser is added to the molten pool. As the laser moves along the scanning direction, the molten pool goes forward synchronously. The molten pool at the back edge of the laser is gradually solidified to form the mushy zone, and then completely changes to a solid state. Therefore, there is a large temperature gradient in the clad parallel to the laser scanning direction, which results in the accumulation of thermal stress.

The temperature, temperature gradient, and stress distribution at different positions of the clad are shown in Fig. 5. On the one hand, the temperature distribution in the molten pool and its vicinity is uneven. Most of the laser energy for laser cladding technology can be assumed to be Gaussian distributed, and the distribution of laser power density at the center and the edge is varied greatly. According to reference [25], the temperature gradient at the edge of the molten pool is about twice as high as that at the center. On the other hand, there are complex convection and heat transfer processes inside the molten pool, resulting in a large temperature gradient along the depth of the molten pool. Furthermore, the size of the molten pool is small relative

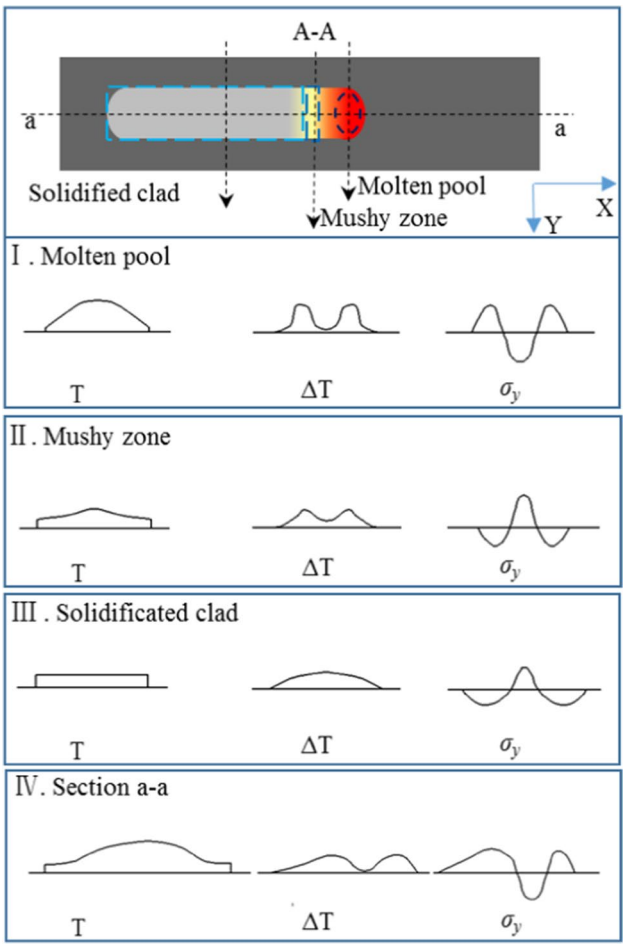

Fig. 5 Schematic of temperature distribution, changes in temperature, and stress of the clad at different zones

to the substrate, which results in a large temperature gradient in and around the molten pool [26]. The distributions of temperature, temperature gradient, and stress state of the clad are shown in Fig. 5. During the phase transformation of solid metal into liquid state, the volume of the liquid metal is expanded. However, the expansion behavior of the molten pool is limited by the H13 substrate. Therefore, there is compressive stress in the molten pool and tensile stress in the surrounding substrate. At the same time, there is a plastic deformation for the material in the molten pool, which would also affect the distribution of thermal stress. In the mushy zone, the solidification phase transformation and volume shrinkage occur. The distribution of temperature, the temperature gradient, and cooling rate within the mushy zone are different. As a result, there is a difference in volume shrinkage between the central and surrounding materials, and the shrinkage behavior of the central material is limited by the surrounding material. Therefore, there is tensile stress in the central material and compressive stress in the surrounding material within the mushy zone. The temperature distribution in the solidified clad region is gradually uniform, resulting in a gradually uniform stress distribution. Additionally, the transformation of the microstructure during the solidification process also causes a volume change, thus causing the accumulation of microstructure stress in the clad.

Therefore, the main reasons for the accumulation of thermal stress in the cladding process are as follows: (1) the irradiation area of the laser is relatively small and the time of melting and solidification process is relatively short, resulting in excessive local temperature and temperature gradient. (2) The laser moves with respect to the substrate during the cladding process, and the position of melting and solidification of the substrate is constantly changing. For a certain point, it undergoes one cycle of melting and solidification process. For the whole substrate, laser cladding is a local melting and solidification process occurring at different locations with continuous, asymmetric cyclic, and temporally ordered characteristics.

The thermal stress in the coating is three-dimensional. To express the stress in different directions conveniently, the coordinate system is established and shown in Fig. 1. The direction along the laser scanning speed is established as the *X*-axis, the direction perpendicular to the laser scanning speed is defined as the *Y*-axis, and the depth direction of molten pool is set as the *Z*-axis. In general, the thermal stress along the *Y*-direction is relatively small, about one to two orders of magnitude lower than that in the other two directions [27–29]. Therefore, the direction of surface crack is perpendicular to the laser scanning direction.

To quantify the relationship between cracks and process parameters, the parameter of crack rate is introduced. The crack rate, which is defined as Eq. (1), is used to evaluate the crack susceptibility of the coating.

$$R = \frac{\sum L_i}{A} \tag{1}$$

where L_i (mm) is the length of the crack, and A (mm^2) is the area of clad surface.

The effect of laser scanning speed on the crack rate is shown in Fig. 6. Under the laser power of 2000 W, the crack rate increases with the increase of laser scanning speed. When the laser power is relatively low and the speed is relatively high, the heated H13 substrate and Ni60 powder are not fully melted, which leads to more defects such as pores, unmelt particles, and slags in the clad. These defects in the clad will cause stress concentration, thus increasing the susceptibility of crack nucleation. At the same time, the plastic flow under high temperature in the molten pool is weakened, resulting in large residual stress accumulated in the clad. When the cladding speed is relatively high, the crack rate is effectively reduced by increasing the laser power. This is because when the laser power increases,

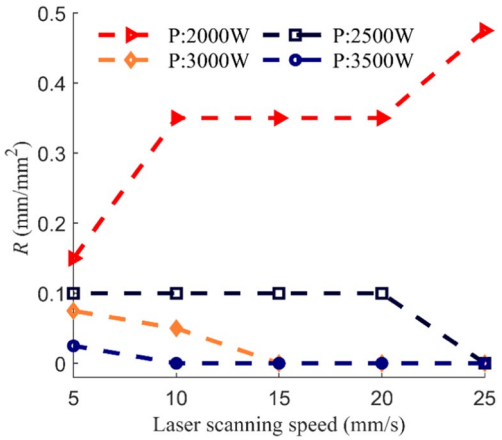

Fig. 6 Relationship between crack rate and laser scanning speed under different laser powers in single-track cladding

the temperature and fluidity of the molten pool increase correspondingly, which is conducive to the homogeneous melting of the materials. In addition, the cladding material is a self-fluxing powder. Therefore, the high temperature of the molten pool is conducive to the precipitation of impurities, thus reducing the cracking tendency of the clad.

The surface crack morphology and the crack morphology inside the clad and the substrate under different laser powers and scanning speed are shown in Figs. 7 and 8, respectively. To clearly show the state of surface crack and its behavior along the depth direction of the molten pool, the morphologies of crack propagation in the substrate and the clad are shown in Fig. 9. The surface crack propagates along the direction parallel to the *Z*-axis until to the substrate, thus inducing cracks in the substrate. According to Fig. 9b, the characteristics of trans-granular fracture are shown from the crack propagation in the *Z*-direction.

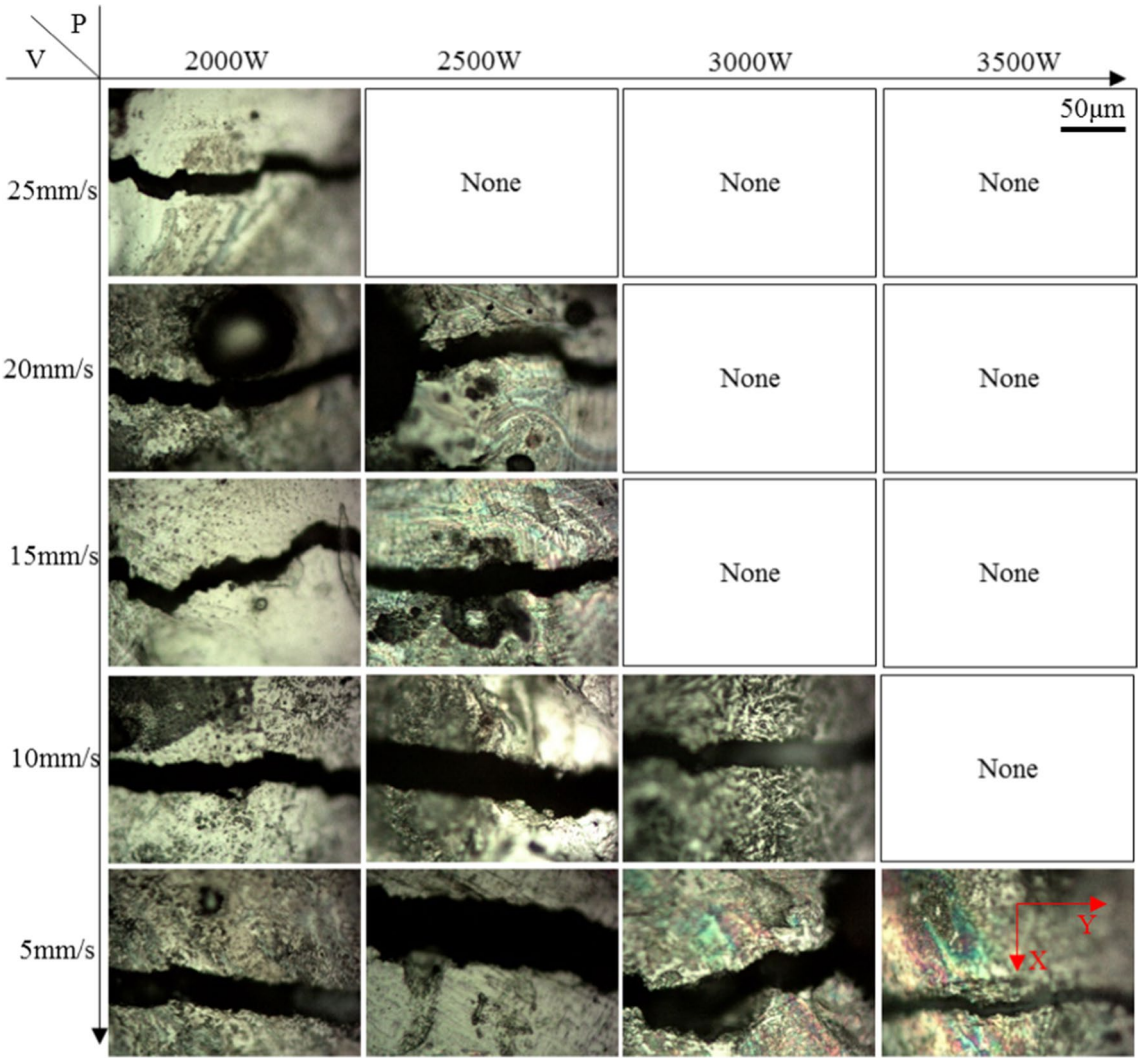

Fig. 7 Crack morphology in *XY* plane under different laser powers and scanning speed in single-track cladding

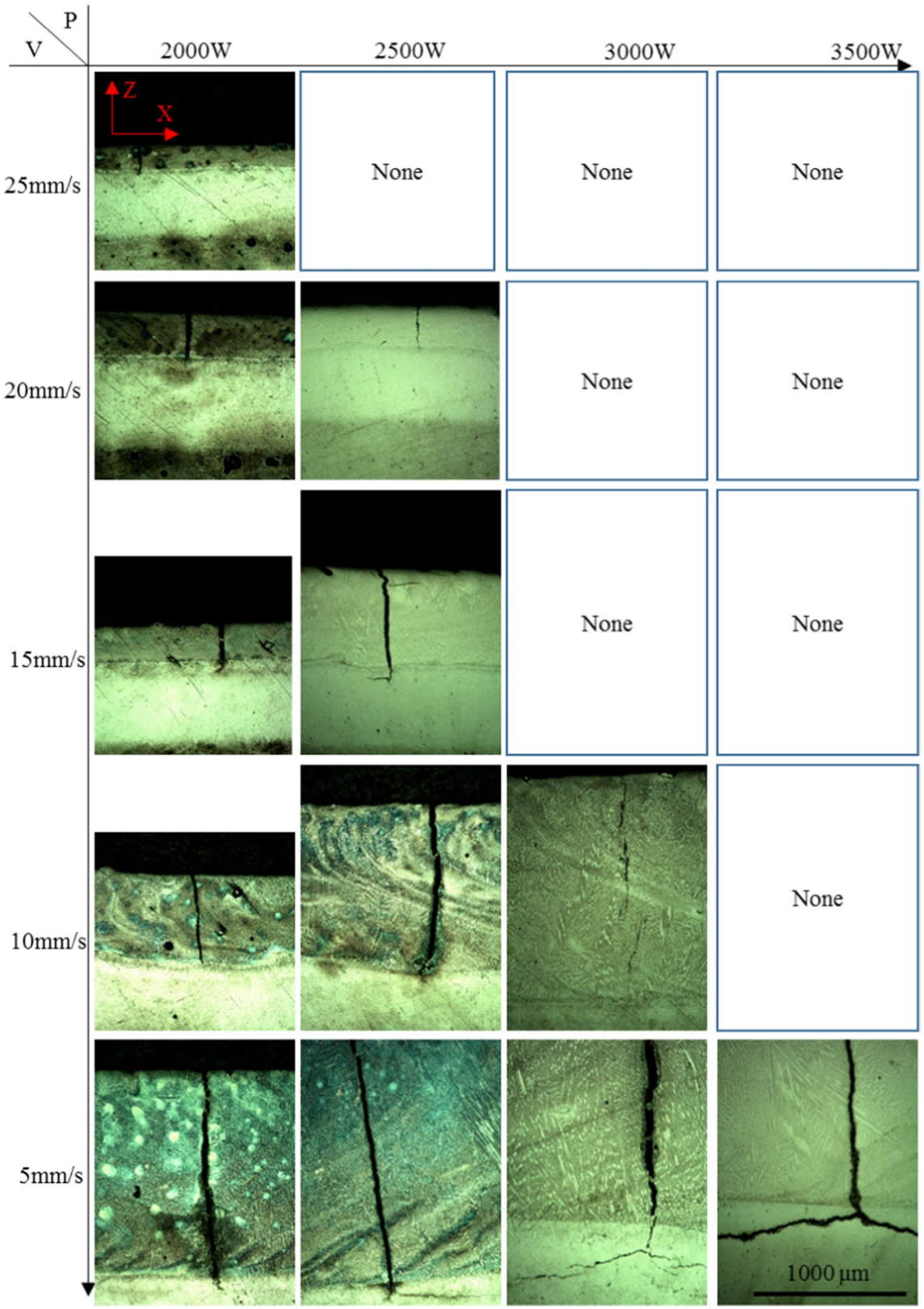

Fig. 8 Crack morphology in *XZ* plane under different laser powers and scanning speed in single-track cladding

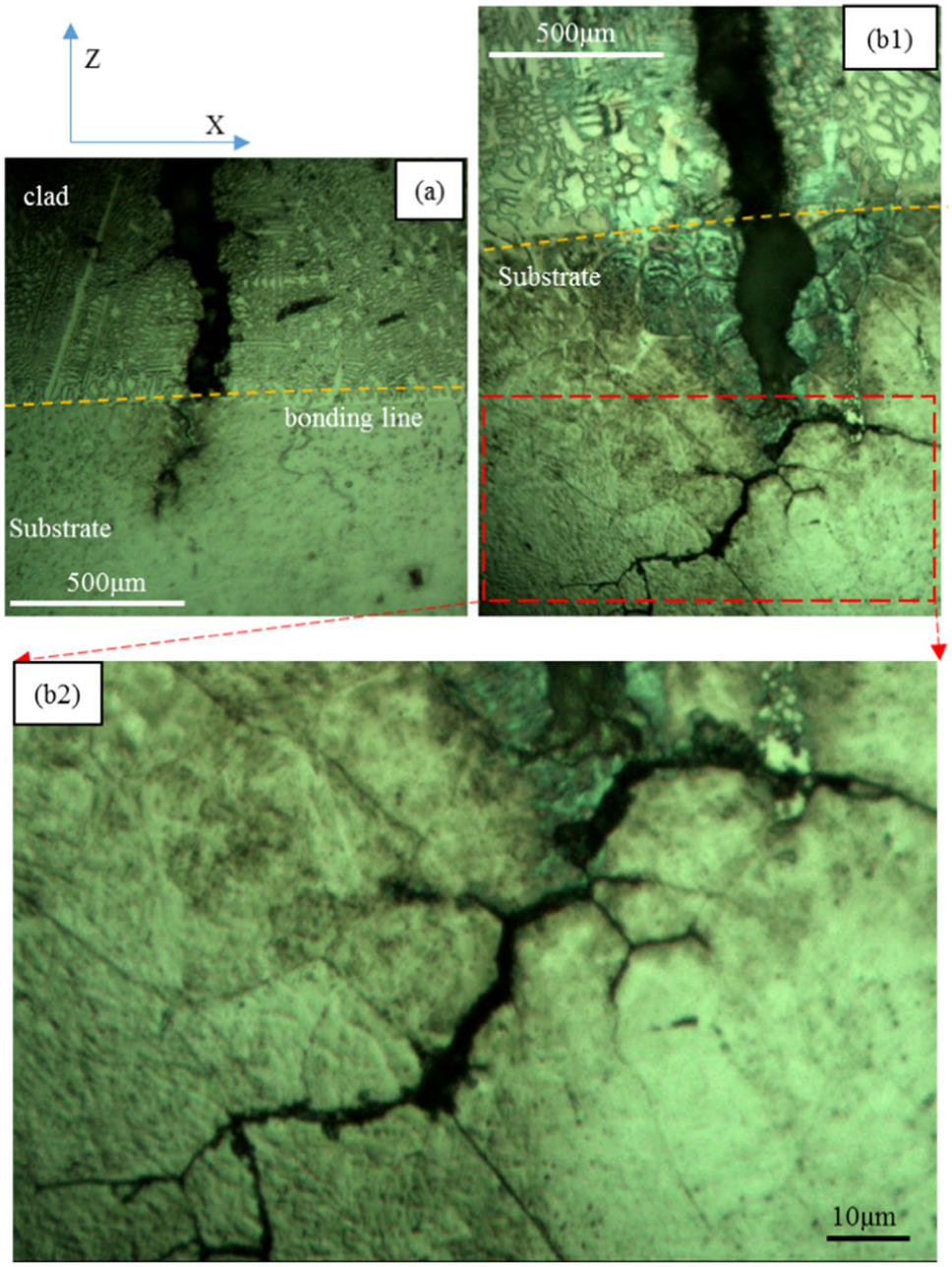

Fig. 9 Crack propagation in single-track cladding: (**a**) along *Z*-direction in substrate under laser power of 2000 W and laser scanning speed of 15 mm/s, (b1, b2) along *X*- and *Z*-direction in substrate under laser power of 2500 W and laser scanning speed of 5 mm/s

The influence of processing parameters on crack evolution is mainly reflected in two aspects: (1) the processing parameters affect the size of the crack, as shown by the increase in crack width and crack length with increasing laser power. Under laser power of 3500 W and scanning speed of 5 mm/s, the crack in the substrate along the *X*-direction is the longest. The crack length is about 3 mm in the *X*-negative direction and 5.1 mm in the *X*-positive direction. (2) Under different laser powers and scanning speed, the direction for crack propagation in the substrate is different. It is shown that when the laser power is relatively low and the speed is relatively high, the crack in the substrate tends to propagate only in the *Z*-direction. When the laser power is relatively high and the scanning speed is relatively low, the crack will continue to propagate along the *X*-direction at the end of the crack in the *Z*-direction and secondary cracks form. According to Fig. 9b, the characteristics of transgranular fracture are shown from the crack propagation in the *X*-direction.

According to the crack location and propagation direction, the single-track clad can be divided into three types: the clad without cracks (NC), the clad with cracks propagating along the *Z*- and *X*-directions (C_ZX), and

the clad with cracks propagating along the *Z*-direction (C_Z). The relationship between these three states and processing parameters is shown in Fig. 10. As can be seen from Fig. 10, when the laser power and the scanning speed are relatively high, the cladding layer under such processing parameters is free from cracks.

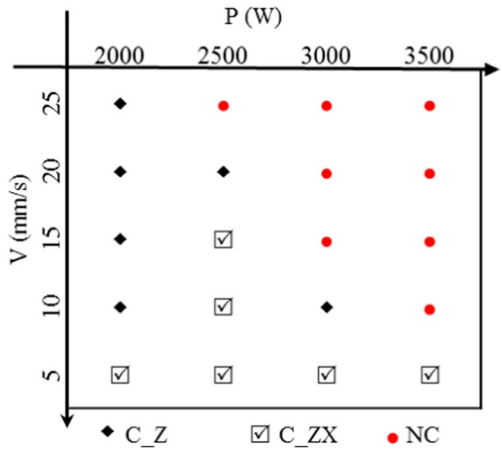

Fig. 10 State diagram for crack evolution in single-track cladding

3.2 Mechanism for crack initiation and propagation in single-track clads

Figure 11 shows the mechanism of crack initiation and propagation. In laser cladding process, the heat energy is accumulated on the surface of the clad and transferred to the interior of the coating by means of heat conduction and convection. As a result, the temperature and temperature gradient on the surface of the clad are higher than the interior materials. In the solidification process, the heat energy is dissipated by way of forced convection and thermal radiation, resulting in a higher cooling rate at the surface of the clad. The temperature gradient and cooling rate are the main factors affecting the crack nucleation. Therefore, cracks are easy to initiate on the surface (shown as point M in Fig. 11b).

Figure 11a shows the stress analysis in the coating in the *XZ* plane. The tensile residual stress σ_x along the *X*-axis direction is unevenly distributed from the upper surface of the clad to the substrate. According to the stress principle, the crack propagates in the direction perpendicular to the principal stress. Therefore, when the residual tensile stress σ_x is greater than the fracture toughness of the material σ^c, the crack propagates in the coating along the *Z*-direction (as shown in Fig. 11c).

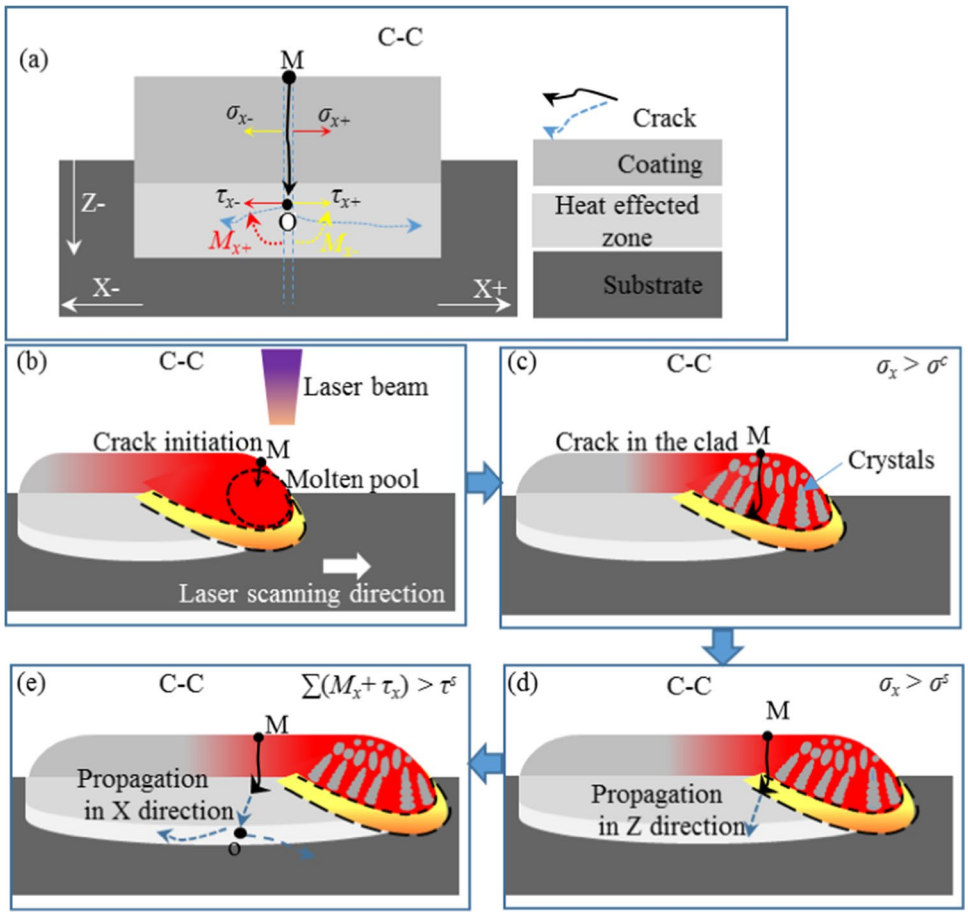

Fig. 11 (**a**) Schematic diagram of stress in the clad and substrate, (**b**) ~ (**e**) mechanism of crack initiation and propagation

The microstructure at the bottom, middle, and top of the cross-section under laser power of 3000 W and scanning speed of 10 mm/s is shown in Fig. 12. It can be seen that the microstructure of the coating consists of dendrites and inter-dendrite network of the substrate. At the bottom of the coating, it is mainly composed of columnar crystals and cellular crystals. During the solidification process, a typical dendritic growth occurs in the middle of the clad, with the formation of large-sized columnar grains. Quick heat dissipation occurs at the top of the clad, which leads to a relatively fine equiaxed crystal structure. This typical growth mode of crystal growth in the clad provides a path for crack propagation.

In the cladding process, the residual tensile stress in the coating is further accumulated, when it exceeds the fracture toughness of the substrate σ^s, and the crack will continue to propagate along the *Z*-direction towards the interior of the substrate (as shown in Fig. 11d). Cracks in the H13 substrate propagate along the inter-granular path (as shown in Fig. 9(b2)). When the laser power is relatively high and the scanning speed is relatively small, crack propagation along the *X*-direction is found in the substrate. The crack propagation along the *X*-direction is located in the heat-affected zone (HAZ), rather than the bonding position of the substrate and the clad, indicating that the bonding strength of the substrate and the clad is greater than the strength of the substrate itself.

The propagation process of cracks in the substrate along the *X*-direction is shown in Fig. 11e. According to the principle of force balance, there is a balance between the bending moment M_x and shear stress τ_x at the point O within the substrate with the force of σ_x. When the resultant force of the bending moment M_x and the shear stress τ_x is greater than the shear strength of the substrate τ^s, the substrate is torn along the *X*-direction, which is manifested by the crack continuing to propagate along the *X*-direction in the substrate.

3.3 Morphology and characteristics of cracks in multi-track clads

The overlapping process is a very important step, and overlapping parameters affect the thermal process in laser cladding. Therefore, the overlapping ratio δ, which is defined as the ratio of the overlap width of two adjacent clads d to the width of single-track clad W, is introduced:

$$\delta = \frac{d}{W} \tag{2}$$

To study the dynamic evolution behavior of the crack in multi-track overlapping process, the multi-track cladding experiments were carried out with laser power of 2500 W, 3000 W, and 3500 W, laser scanning speed of 20 mm/s, and overlap ratio of 0.4. The surface crack morphology after dye penetration test is shown in Fig. 13. It can be clearly seen that the number and morphology of cracks vary greatly under different laser powers. When the laser power is 2500 W, the number of surface cracks is the largest and the cracks are distributed in a network pattern. When the laser power is 3000 W and 3500 W, only transverse cracks appear on the surface of the clad, and the number of cracks is reduced significantly. The relationship between the laser power and the crack rate in multi-track cladding is shown in Fig. 14. Under the laser power of 2500 W and the scanning speed of 20 mm/s, the crack rate in the multi-track clads is 0.5 mm/mm^2, which is much greater than that in the single-track clad under the same laser power and laser scanning speed.

Figure 15 shows the surface crack morphology at different magnifications under different laser powers. Figure 16 shows the crack morphology in the *XZ* and *YZ* planes under the laser power of 2500 W, and Fig. 17 shows the crack

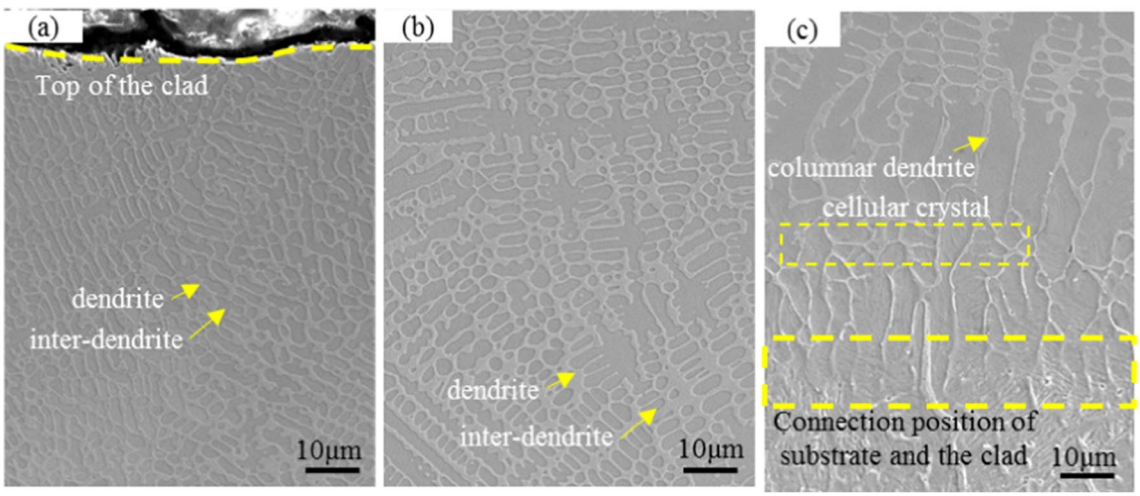

Fig. 12 Cross-sectional micrographs of the clad under laser power of 3000 W and scanning speed of 10 mm/s (**a**) top, (**b**) middle, (**c**) bottom

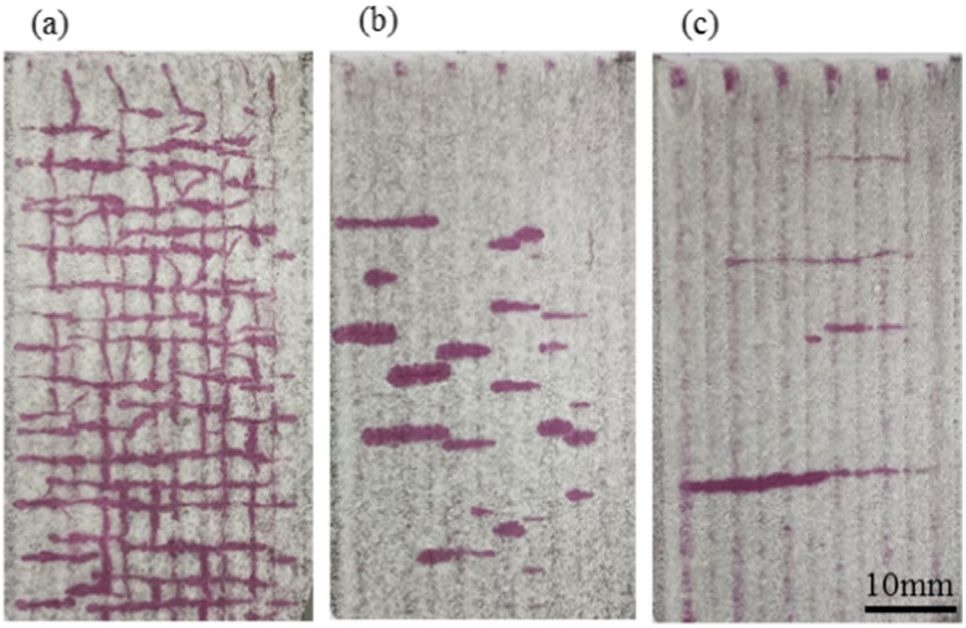

Fig. 13 Surface crack morphology in multi-track clads under scanning speed of 20 mm/s and laser power of (**a**) 2500 W, (**b**) 3000 W, (**c**) 3500 W

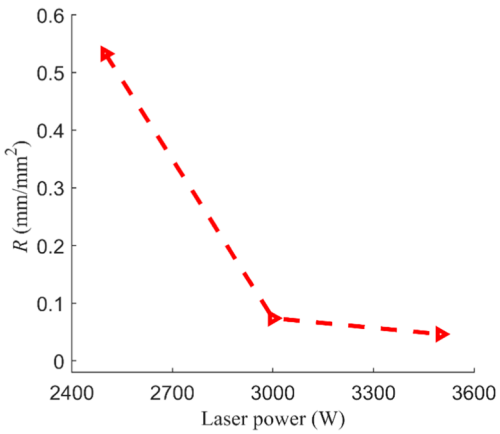

Fig. 14 Relationship between crack rate and laser power for multi-track clads under scanning speed of 20 mm/s

morphology in the depth direction under the laser power of 3000 W and 3500 W. It can be clearly seen from Fig. 15 that the surface of the clad is not smooth due to the bonding of un-melted particles. When the laser power is relatively low (2500 W), the distribution of un-melted particles on the whole cladding surface is relatively uniform. With the increase of laser power, the distribution of the un-melted particles tends to be more uneven, which is manifested by more particles located at the overlap of two adjacent tracks, and fewer particles distributed in the middle of the clads. Furthermore, it is obvious that the number of un-melted particles decreases with the increase of laser power. This is because the temperature of the molten pool increases with the increase of laser power, which leads to more sufficient heating of the materials and a decrease in the number of un-melted particles. Under the laser power of 2500 W, longitudinal cracks parallel to the laser scanning direction appear at the overlap of two adjacent tracks. The longitudinal cracks propagate in the *X*-direction and intersect with transverse cracks successively, resulting in a network distribution for surface cracks.

There are two main reasons for crack propagation along the *X*-direction: (1) Due to the relatively low temperature, short existence time, and weak fluidity at the edge of the melt pool, defects such as porosity, unmelted particles, and slag are easier to occur in the overlapping zone, thus causing the concentration of residual stress. (2) During multi-track cladding, the material in the overlapping zone remelts, resulting in a more complex thermal stress process, which increases the susceptibility to crack initiation.

Under the laser power of 3000 W and 3500 W, no longitudinal cracks are detected in the overlapping zone, and transverse cracks pass through multiple tracks along the direction perpendicular to the laser scanning speed. Therefore, it can be inferred that the initiation and propagation of longitudinal cracks did not take place in the process of multi-track overlapping, and the propagation behavior of cracks in single-track clad is inherited in multi-track cladding process.

It is worth noting that under the laser power of 3000 W and 3500 W, there is no crack initiation in the single-track clad. In the multi-track cladding process with the same laser power and overlapping rate of 0.4, cracks perpendicular to the laser scanning direction could be induced. Under the laser power of 2500 W, the crack direction on the surface for single-track clad is perpendicular to the laser scanning direction, while surface cracks in multi-track clads are distributed in a network pattern. Therefore, in the process of

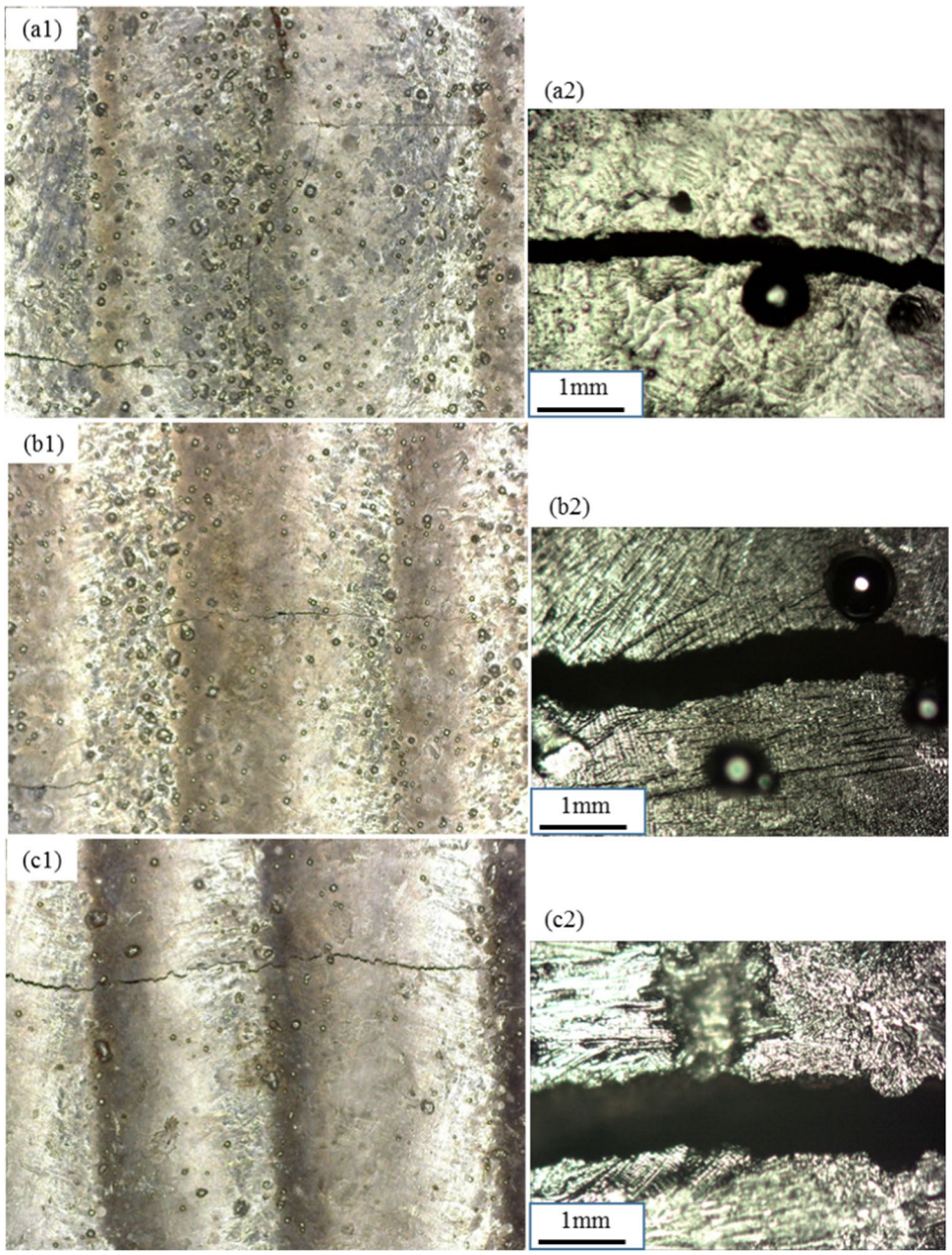

Fig. 15 Surface crack morphology for multi-track clads under laser power of (**a**) 2500 W, (**b**) 3000 W, (**c**) 3500W

laser additive manufacturing, different crack propagation behaviors occur in dynamic process from single-track to multiple-track cladding.

Under the laser power of 2500 W, the propagation direction of cracks in the *XZ* plane is almost parallel to the *Z*-axis, and cracks in the substrate are initiated in multi-track cladding. The cracks in the *YZ* plane are initiated at the overlap of two adjacent tracks, and their propagation direction is closely related to the position of defects in the coating. With the increase of laser power, the behavior of crack propagation varies considerably in multi-track cladding process. Under the laser power of 3000 W and 3500 W, the propagation process of crack in multi-track clads along the depth direction, as shown in Fig. 17, is similar to that in single-track clad, and the propagation direction is almost parallel to the *Z*-axis. The crack in the substrate propagates in the direction parallel to the *Z*-axis and along the *X*-axis in the heated zone, which is manifested as the substrate being torn.

3.4 Mechanism for crack initiation and propagation in multi-track clads

The formation process of transverse cracks and network-shaped cracks in the multi-track cladding process is shown in Fig. 18. As shown in Section 3.1, during the single-track

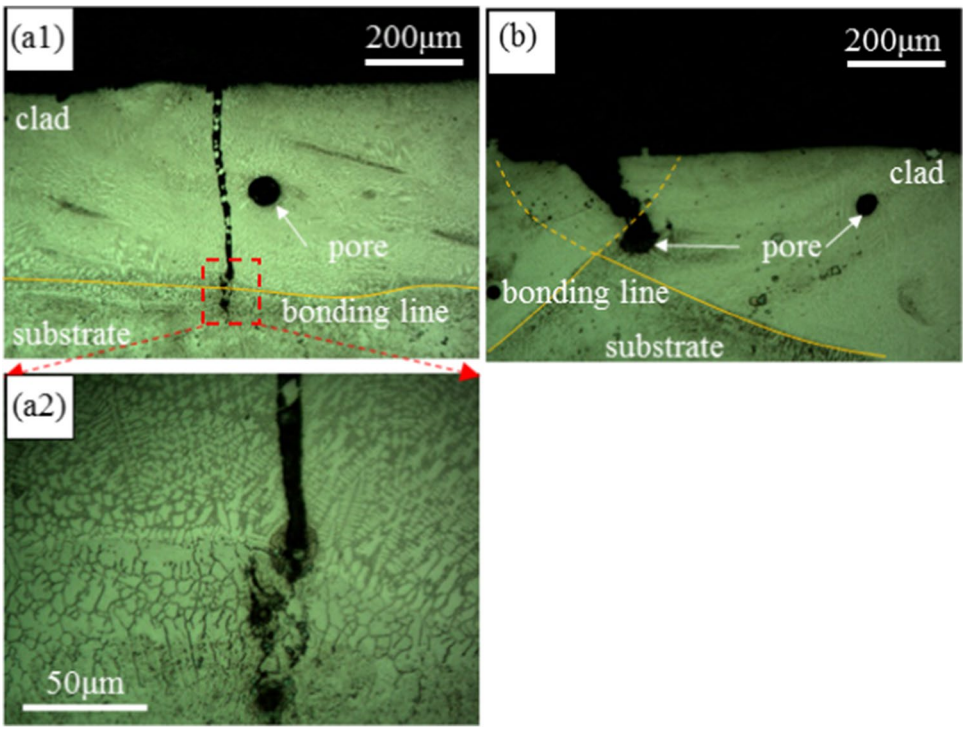

Fig. 16 Crack morphology in multi-track cladding under laser power of 2500 W in (a1, a2) *XZ* plane, (**b**) *YZ* plane

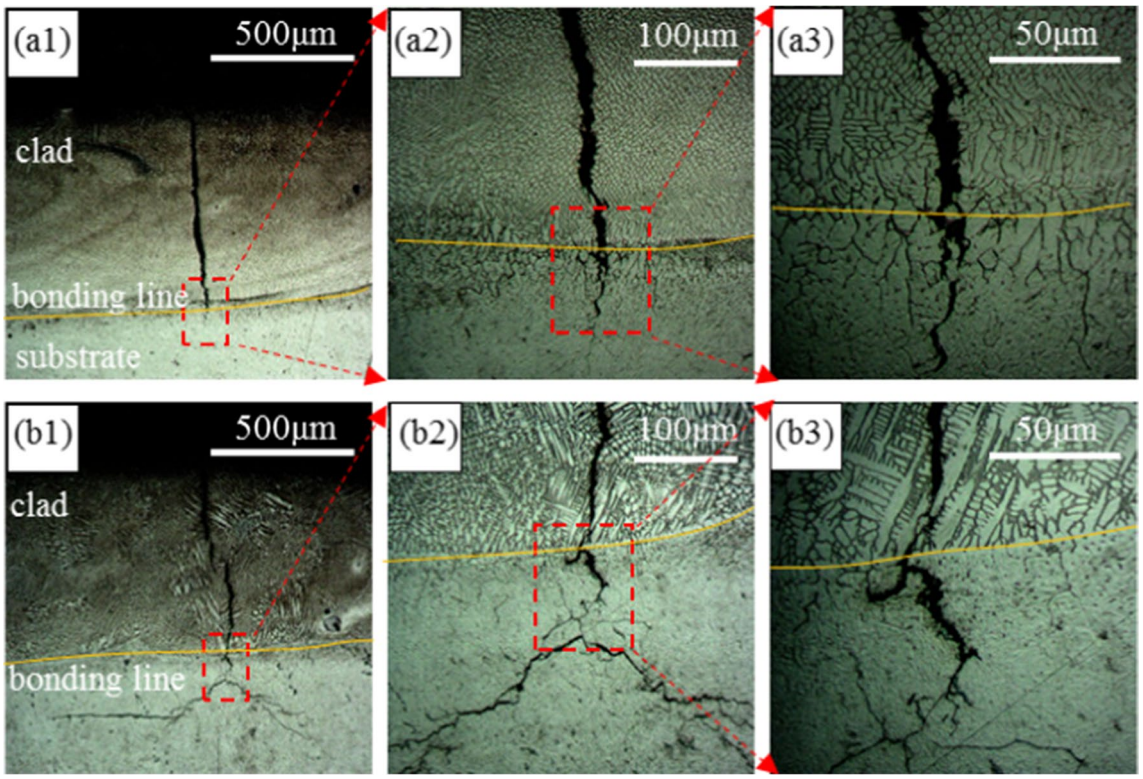

Fig. 17 Crack morphology in multi-track cladding in *XZ* plane under laser power of (**a**) 3000 W, (**b**) 3500 W

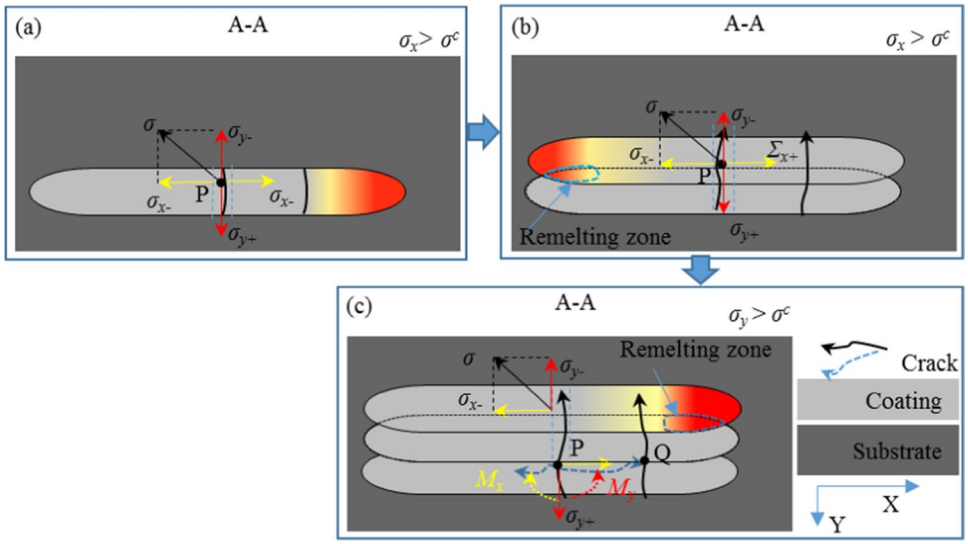

Fig. 18 (**a**~**c**) Schematic diagram of mechanism of crack initiation and propagation in *XY* plane

cladding process, three-dimensional stress in the clad is mainly manifested as the tensile stress σ in the *XY* plane (as shown in Fig. 18a). The components of σ in the *X*- and *Y*-directions are σ_x and σ_y, respectively. When the stress in the *X*-direction σ_x is greater than the fracture toughness of the clad σ^c, transverse cracks appear on the surface of single-track clad. As shown in Fig. 18b, in the process of overlapping cladding, there is a more complex melting-solidification process, which makes the stress σ_x accumulate further. Based on the position of the crack in the previous track, the crack propagates further so that the transverse crack on the surface passes through multiple adjacent tracks. Meanwhile, when the stress in the *Y*-direction σ_y exceeds the fracture toughness of the clad σ^c, the surface crack will

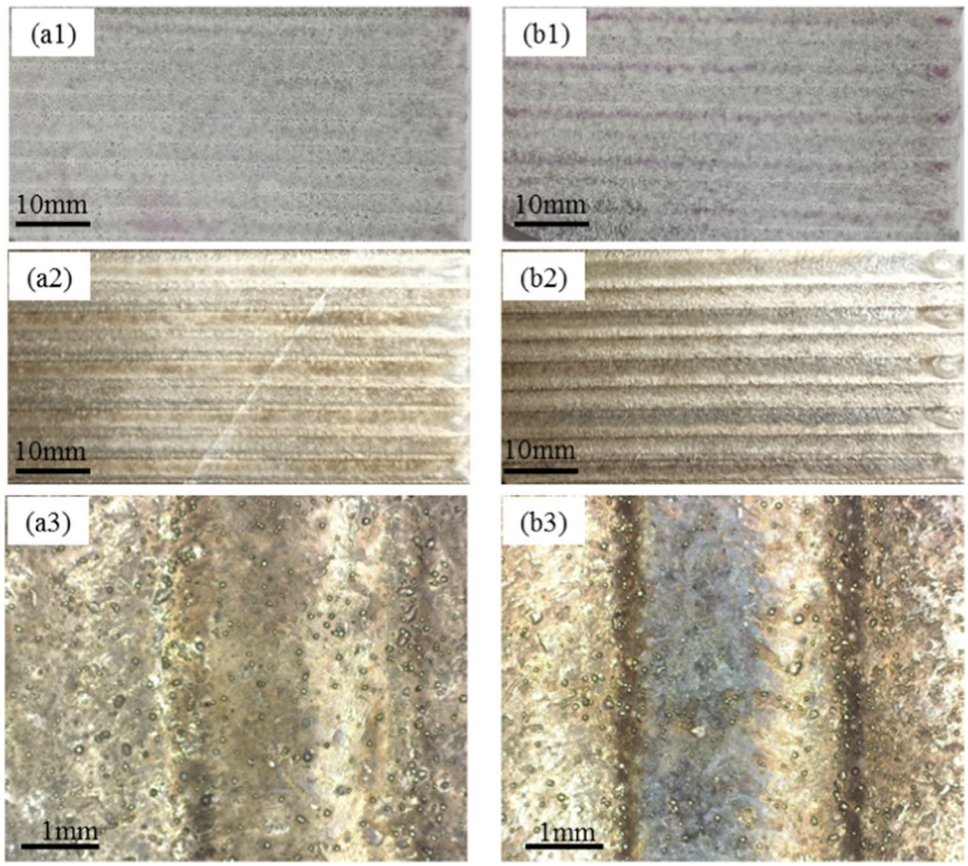

Fig. 19 Crack-free surface morphology in multi-track cladding under laser power of (**a**) 3000 W, (**b**) 3500 W. (a1, b1) Surface morphology after dye penetration test. (a2, b2) Surface morphology before dye penetration test. (a3, b3) Surface morphology in lager magnification

initiate and propagate along the *X*-direction. In multi-track cladding process, more residual stress can be accumulated at the overlapping zone of two adjacent tracks due to the re-melting process. As a result, the cracks in the *X*-direction are mostly found in the overlapping zone.

3.5 Realization of crack-free clads

Overlapping rate is the key processing parameter in multi-track cladding, which determines the thermal history of the material and subsequently effects the evolution and distribution of residual stress in the multi-track clads. With the overlapping rate adjusted to 0.3, the multi-track cladding experiments were carried out under the laser power of 3000 W and 3500 W and the scanning speed of 20 mm/s. The surface morphology of multi-track cladding after dye penetration test and the actual samples are shown in Fig. 19. It can be clearly seen that there are no cracks on the surface of the clad, and the un-melted particles are evenly distributed on the clad surface.

4 Conclusion

In this study, the single-track and multi-track laser cladding experiments of Ni60 alloy powder on H13 substrate have been conducted. The initiation and dynamic evolution behavior of cracks in additive manufacturing process has been investigated. The following conclusions have been drawn:

1. Laser power and scanning speed are the key factors affecting the formation of crack in single-track clad. When the laser power is relatively high and the scanning speed is relatively large, the process range for crack-free clads can be achieved.
2. The effect of scanning speed on crack rate in single-track clad under different laser powers is inconsistent. When the laser power is relatively low, the crack rate increases with the increase of scanning speed. When the laser power is relatively high, the effect of the scanning speed on the crack rate is the opposite.
3. The crack propagation behavior in the substrate is closely related to laser scanning speed. When the scanning speed is relatively large, the crack propagates along the depth direction in the substrate. When the scanning speed is relatively small, the crack propagates in the laser scanning direction in the heat-affected zone along the inter-granular path. Under laser power of 3500 W and scanning speed of 5 mm/s, the crack in the substrate along the *X*-direction is the longest. The crack length is about 3 mm in the *X*-negative direction and 5.1 mm in the *X*-positive direction.
4. Overlapping rate is the key to affect the crack initiation and propagation in multi-track cladding process. The surface cracks in multi-track clads are mainly distributed in network and transverse pattern. The crack-free multi-track cladding can be achieved under laser power of 3000 W and 3500 W, laser scanning speed of 20 mm/s, and overlapping rate of 0.3.

Author contribution Yanhua Bian: data curation, investigation, methodology, roles/writing — original draft; Binxin Dong: investigation, validation, data curation; Bo Chen: data curation, visualization, investigation; Jianhao Guo: validation, methodology, software; Shaoxia Li: formal analysis, validation, funding acquisition; Chongxin Tian: formal analysis, methodology, visualization; Shouwen Xu: visualization, data curation; Xiuli He: project administration, conceptualization, supervision, writing — review and editing; Gang Yu: project administration, conceptualization, funding acquisition, resources.

Funding This work was supported by the National Natural Science Foundation of China (Nos. 11502269 and 11672304) and plan of Beijing Municipal Commission of Science and Technology (No. Z181100003818015).

Data availability The authors confirm that the data supporting the findings of this study are available within the article. The raw data that support the findings of this study are available from the corresponding author, upon a reasonable request.

Code availability Not applicable

Declarations

Ethics approval The research does not involve human participants or animals, and the authors warrant that the paper fulfills the ethical standards of the journal.

Consent to participate It is confirmed that all the authors are aware and satisfied of the authorship order and correspondence of the paper.

Consent for publication The manuscript is approved by all authors for publication; all the authors listed have approved the manuscript that is enclosed.

Competing interests The authors declare no competing interests.

References

1. Narvan M, Al-Rubaie KS, Elbestawi M (2019) Process-structure-property relationships of AISI H13 tool steel processed with selective laser melting. Materials 12(14):2284. https://doi.org/10.3390/ma12142284
2. Wei MX, Wang SQ, Wang L, Cui X, Chen KM (2011) Effect of tempering conditions on wear resistance in various wear mechanisms of H13 steel. Tribol Int 44(7–8):898–905. https://doi.org/10.1016/j.triboint.2011.03.005
3. Cong DL, Zhou H, Ren ZN, Zhang Z, Zhang H, Meng C, Wang C (2014) The thermal fatigue resistance of H13 steel repaired

by a biomimetic laser remelting process. Mater Des 55:597–604. https://doi.org/10.1016/j.matdes.2013.09.076
4. Arias-Gonzalez F, del Val J, Comesana R, Penide J, Lusquiños F, Quintero F, Riveiroa A, Boutinguizaa M, Pou J (2016) Fiber laser cladding of nickel-based alloy on cast iron. Appl Surf Sci 374:197–205. https://doi.org/10.1016/j.apsusc.2015.11.023
5. Li WY, Yang XF, Xiao JP, Hou QM (2021) Effect of WC mass fraction on the microstructure and friction properties of WC/Ni60 laser cladding layer of brake discs. Ceram Int 47(20):28754–28763. https://doi.org/10.1016/j.ceramint.2021.07.035
6. Ahn DG (2021) Directed energy deposition (DED) process: state of the art. Int J Pr Eng MAN-GT 8(2):703–742. https://doi.org/10.1007/s40684-020-00302-7
7. Guan XY, Zhao YF (2020) Modeling of the laser powder-based directed energy deposition process for additive manufacturing: a review. Int J Adv Manuf Tech 107(5–6):1959–1982. https://doi.org/10.1007/s00170-020-05027-0
8. Ahmed N (2019) Direct metal fabrication in rapid prototyping: a review. J Manuf Process 42:167–191. https://doi.org/10.1016/j.jmapro.2019.05.001
9. Wang WQ, Liu L, Zhang XG, Shi ZM, Tian YT, Lin JX (2020) Microstructures and mechanical properties of Ni60 alloy fabricated by laser metal deposition. Mater Res Express 7(1):016569. https://doi.org/10.1088/2053-1591/ab69c7
10. Li JH, Xue SL, Yao FP, An XJ, Jin JB (2022) Morphology control and process optimization for the laser cladding of Ni60 alloy onto H13 steel. Lasers Eng 52(4–6):261–281
11. Yu T, Deng QL, Dong G, Yang JG (2011) Effects of Ta on microstructure and microhardness of Ni based laser clad coating. Appl Surf Sci 257(11):5098–5103. https://doi.org/10.1016/j.apsusc.2011.01.027
12. Meng L, Sheng PH, Zeng XY (2022) Comparative studies on the Ni60 coatings deposited by conventional and induction heating assisted extreme-high-speed laser cladding technology: formability, microstructure and hardness. J Mater Res Technol 16:1732–1746. https://doi.org/10.1016/j.jmrt.2021.12.110
13. Alizadeh-Sh M, Marashi SPH, Ranjbarnodeh E, Shoja-Razavi R (2020) Laser cladding of Inconel 718 powder on a non-weldable substrate: clad bead geometry-solidification cracking relationship. J Mater Process 56:54–62. https://doi.org/10.1016/j.jmapro.2020.04.045.
14. Fu FX, Zhang YL, Chang GR, Dai J (2016) Analysis on the physical mechanism of laser cladding crack and its influence factors. Optik 127(1):200–202. https://doi.org/10.1016/j.ijleo.2015.10.043.
15. Song MJ, Wu LS, Liu JM, Hu Y (2021) Effects of laser cladding on crack resistance improvement for aluminum alloy used in aircraft skin. Opt Laser Technol 133:106531. https://doi.org/10.1016/j.optlastec.2020.106531
16. Kadolkar PB, Watkins TR, De Hosson JTM, Kooi BJ, Dahotre NB (2007) State of residual stress in laser-deposited ceramic composite coatings on aluminum alloys. Acta Mater 55(4):1203–1214. https://doi.org/10.1016/j.actamat.2006.07.049
17. Zhou SF, Zeng XY, Hu QW, Huang YJ (2008) Analysis of crack behavior for Ni-based WC composite coatings by laser cladding and crack-free realization. Appl Surf Sci 255(5):1646–1653. https://doi.org/10.1016/j.apsusc.2008.04.003
18. Huang YJ, Zeng XY (2010) Investigation on cracking behavior of Ni-based coating by laser-induction hybrid cladding. Appl Surf Sci 256(20):5985–5992. https://doi.org/10.1016/j.apsusc.2010.03.106
19. Lee C, Park H, Yoo J, Lee C, Woo W, Park S (2015) Residual stress and crack initiation in laser clad composite layer with Co-based alloy and WC plus NiCr. Appl Surf Sci 345:286–294. https://doi.org/10.1016/j.apsusc.2015.03.168
20. Wang JD, Li LQ, Tao W (2016) Crack initiation and propagation behavior of WC particles reinforced Fe-based metal matrix composite produced by laser melting deposition. Opt Laser Technol 82:170–182. https://doi.org/10.1016/j.optlastec.2016.03.008
21. Shi BW, Li T, Guo ZW, Zhang XR, Zhang HC (2022) Selecting process parameters of crack-free Ni60A alloy coating prepared by coaxial laser cladding. Opt Laser Technol 149:107805. https://doi.org/10.1016/j.optlastec.2021.107805
22. Zhang Z, Kovacevic R (2019) A thermo-mechanical model for simulating the temperature and stress distribution during laser cladding process. Int J Adv Manuf 102(1–4):457–472. https://doi.org/10.1007/s00170-018-3127-y
23. Sun ST, Fu HG, Chen SY, Ping XL, Wang KM, Guo XY, Lin J, Lei YP (2019) A numerical-experimental investigation of heat distribution, stress field and crack susceptibility in Ni60A coatings. Opt Laser Technol 117:175–185. https://doi.org/10.1016/j.optlastec.2019.04.021
24. Bian YH, He XL, Yu G, Li SX, Tian CX, Li ZY, ZhangYM LJM (2022) Powder-flow behavior and process mechanism in laser directed energy deposition based on determined restitution coefficient from inverse modeling. Powder Technol 402:87355. https://doi.org/10.1016/j.powtec.2022.117355
25. Gan ZT, Yu G, He XL, Li SX (2017) Numerical simulation of thermal behavior and multicomponent mass transfer in direct laser deposition of Co-base alloy on steel. J Heat Mass Transfer 104:28–38. https://doi.org/10.1016/j.ijheatmasstransfer.2016.08.049
26. Griffith ML, Schlienger ME, Harwell LD, Oliver MS, Baldwin MD, Ensz MT, Essien M, Brooks J, Robino CV, Smugeresky JE (1999) Understanding thermal behavior in the LENS process. Mater Des 20(2–3):107–113. https://doi.org/10.1016/S0261-3069(99)00016-3
27. Triantafyllidis D, Li L, Stott FH (2006) Crack-free densification of ceramics by laser surface treatment. Surf Coat Technol 201(6):3163–3173. https://doi.org/10.1016/j.surfcoat.2006.06.032
28. Shen XH, He XP, Gao LY, Su GS, Xu CH, Xu N (2022) Study on crack behavior of laser cladding ceramic-metal composite coating with high content of WC. Ceram Int 48(12):17460–17470. https://doi.org/10.1016/j.ceramint.2022.03.010
29. Zhou SF, Dai XQ (2010) Laser induction hybrid rapid cladding of WC particles reinforced NiCrBSi composite coatings. Appl Surf Sci 256(14):4708–4714. https://doi.org/10.1016/j.msea.2007.07.058